Monthly Notices
of the
ROYAL ASTRONOMICAL SOCIETY

Mon. Not. R. Astron. Soc. **425,** 2576–2588 (2012) doi:10.1111/j.1365-2966.2012.21739.x

V496 Scuti: an Fe II nova with dust shell accompanied by CO emission

Ashish Raj,[1⋆] N. M. Ashok,[1] D. P. K. Banerjee,[1] U. Munari,[2] P. Valisa[3] and S. Dallaporta[3]

[1]*Astronomy and Astrophysics Division, Physical Research Laboratory, Navrangpura, Ahmedabad-380009, Gujarat, India*
[2]*INAF Astronomical Observatory of Padova, 36012 Asiago (VI), Italy*
[3]*ANS Collaboration, c/o Osservatorio Astronomico, via dell'Osservatorio 8, 36012 Asiago (VI), Italy*

Accepted 2012 July 18. Received 2012 July 18; in original form 2012 April 16

ABSTRACT

We present near-infrared (near-IR) and optical observations of the nova Scuti 2009 (V496 Sct) covering various phases – pre-maximum, early decline and nebular – during the first 10 months of its discovery followed by limited observations in the early part of 2011 April. The spectra follow the evolution of the nova when the lines had strong P Cygni profiles to a phase dominated by prominent emission lines. The notable feature of the near-IR spectra in the early decline phase is the rare presence of first overtone bands of carbon monoxide in emission. Later about 150 days after the peak brightness, the IR spectra show clear dust formation in the expanding ejecta. Dust formation in V496 Sct is consistent with the presence of lines of elements with low ionization potentials like Na and Mg in the early spectra and the detection of CO bands in emission. The light curve shows a slow rise to the maximum and a slow decline indicating a prolonged mass loss. This is corroborated by the strengthening of P Cygni profiles during the first 30 days. In the spectra taken close to the optical maximum brightness, the broad and single absorption components seen at the time of discovery are replaced by two sharper components. During the early decline phase, two sharp dips that show increasing outflow velocities are seen in the P Cygni absorption components of Fe II and H I lines. The spectra in 2010 March showed the onset of the nebular phase. Several emission lines display saddle-like profiles during the nebular phase. In the nebular stage, the observed fluxes of [O III] and Hβ lines are used to estimate the electron number densities and the mass of the ejecta. The optical spectra show that the nova is evolved in the $P_{\rm fe}A_{\rm o}$ spectral sequence. The physical conditions in the ejecta are estimated. The absolute magnitude and the distance to the nova are estimated to be $M_V = -7.0 \pm 0.2$ and $d = 2.9 \pm 0.3$ kpc, respectively.

Key words: line: identification – techniques: spectroscopic – stars: individual: V496 Sct – novae, cataclysmic variables.

1 INTRODUCTION

Nova Scuti 2009 (V496 Sct) was discovered by Nishimura on 2009 November 8.370 UT at $V = 8.8$ (Nakano 2009). The low-resolution spectra obtained soon after its discovery in the period 2009 November 9.73 UT to 10.08 UT showed prominent Hα and Hβ emission lines with P Cygni components, along with the strong Fe II multiplets and O I lines indicating that V496 Scuti is an Fe II class nova near the maximum light (Balam & Sarty 2009; Munari et al. 2009a; Teyssier 2009). The typical full width at half-maximum (FWHM) of the P Cygni components ranged from 700 to 950 km s^{-1} with the absorption component blueshifted by 700 km s^{-1}. The follow-up observations by Munari et al. (2009b) showed a post-discovery brightening for about 10 days before the onset of fading with the maximum brightness $V_{\rm max} = 7.07$ around 2009 November 18.716 UT. V496 Sct was observed in the infrared (IR) by Rudy et al. (2009) using Near-Infrared Imaging Spectrograph on the 3-m Shane reflector at the Lick Observatory on 2009 November 27.08 UT and revealed a strong first overtone CO emission – an extremely short-lived feature that is seen in only a few novae. They also found several prominent C I emission lines with the strongest line accompanied by P Cygni type absorption component. As the novae that display first overtone CO in emission and strong C I emission in early phases form dust, Rudy et al. (2009) predicted that dust formation in V496 Sct is almost certain. Following this interesting prediction, an observational campaign of V496 Sct was initiated at Mt. Abu IR Observatory and the first result by Raj, Ashok & Banerjee (2009) showed the

⋆E-mail: ashishr@prl.res.in

continuation of CO emission during the period 2009 December 3.55–8.55 UT. Subsequent observations by Russell et al. (2010) after V496 Sct came out of the solar conjunction showed dust formation on 2010 February 10. The CO emission seen in 2009 November was absent.

An inspection by Guido & Sostero (2009) of the Digitized Sky Survey (DSS) plate (limiting red magnitude of about 20) obtained on 1996 August 13 did not reveal any clear and unambiguous object at the position of V496 Sct. The limiting red magnitude of 20 for the DSS plate makes V496 Sct one of the large amplitude ($\Delta R \geq 13.5$) novae.

The nova V496 Sct was studied at Mt. Abu IR Observatory of Physical Research Laboratory in India, at Asiago Observatory operated by the University of Padova and INAF Astronomical Observatory of Padova and Schiaparelli Observatory in Italy. In this paper, we present spectral evolution during the pre-maximum rise, early decline and the nebular phase.

2 OBSERVATIONS

2.1 Infrared observations

Near-IR observations were obtained using the 1.2-m telescope of Mt. Abu IR Observatory from 2009 November 19 to 2011 April 23. The availability of V496 Sct for short duration during 2009 December resulted in restricted photometric coverage. The log of the spectroscopic and photometric observations is given in Table 1. The spectra were obtained at a resolution of ∼1000 using a Near-Infrared Imager/Spectrometer with a 256 × 256 HgCdTe NICMOS3 array. In each of the *JHK* bands, a set of spectra was taken with the nova offset to two different positions along the slit (slit width = 1 arcsec). The wavelength calibration was done using the OH sky lines that register with the stellar spectra. The spectra of the comparison stars SAO 144150 (spectral type B9.5 III) and SAO 142612 (spectral type B9) were taken at a similar airmass as that of V496 Sct to ensure that the ratioing process (nova spectrum divided by the standard star spectrum) removes the telluric features reliably. To avoid artificially generated emission lines in the ratioed spectrum, the H I absorption lines in the spectra of standard star were removed by interpolation before ratioing. The ratioed spectra were then multiplied by a blackbody curve corresponding to the standard star's effective temperature to yield the final spectra.

Photometry in the *JHK* bands was done in clear sky conditions using the NICMOS3 array in the imaging mode. Several frames, in four dithered positions, offset by ∼30 arcsec were obtained in all the bands. The sky frames, which are subtracted from the nova frames, were generated by median combining the dithered frames. The star SAO 142612 having Two Micron All Sky Survey *JHK* magnitudes of 6.55, 6.51 and 6.44, respectively, and located close to the nova was used for photometric calibration. The data are reduced and analysed using the IRAF package.

2.2 Optical photometry

Optical photometry of V496 Sct was obtained with ANS Collaboration telescope number R030 located in Cembra (Trento, Italy). A detailed description of ANS Collaboration instruments, operation modes and results on the monitoring of novae is provided by Munari et al. (2012) and Munari & Moretti (2012). Telescope R030 is a 0.30-m Meade RCX-400 $f/8$ Schmidt–Cassegrain telescope, equipped with a SBIG ST-9 CCD camera, 512 × 512 array, 20-μm pixels ≡ 1.72 arcsec pixel^{-1}, providing a field of view of 13 arcmin × 13 arcmin. The *B* filter is from Omega and the UVR_CI_C filters are from Custom Scientific. The BVR_CI_C photometry of V496 Sct is presented in Table 2. The median values for the total error budget are $\sigma(V) = 0.008$, $\sigma(B-V) = 0.014$, $\sigma(V-R) = 0.012$ and $\sigma(V-I) = 0.027$, which include both the Poissonian components and the uncertainty in the transformation from the local to the standard Landolt (1992) system.

2.3 Optical spectroscopy

Spectroscopic observations of V496 Sct were obtained with the 0.6-m telescope of the Schiaparelli observatory in Varese, equipped with a multimode spectrograph (Echelle + single dispersion modes) and various reflection gratings, as part of the ANS Collaboration monitoring of nova outbursts (Munari et al. 2012). A journal of the spectroscopic observations is provided in Table 3, where the time is counted from the *V*-band maximum. The resolving power of the Echelle spectra is ∼20 000. The spectra were exposed with a

Table 1. Log of the Mt. Abu near-IR observations of V496 Sct. The date of optical maximum is taken as 2009 November 18.716 UT.

Date of observation	Days since optical maximum	Integration time (s)			Integration time (s)			Nova magnitude		
		J band	*H* band	*K* band	*J* band	*H* band	*K* band	*J* band	*H* band	*K* band
		spectroscopic observations			photometric observations					
2009 Nov 19.57	0.854	60	–	–	10	25	50	5.49 ± 0.02	5.20 ± 0.02	4.96 ± 0.10
2009 Dec 03.58	14.864	–	–	60	–	–	–	–	–	–
2009 Dec 05.56	16.844	60	60	120	–	–	–	–	–	–
2009 Dec 06.56	17.844	90	60	120	5	10	10	6.50 ± 0.16	5.82 ± 0.21	5.21 ± 0.14
2009 Dec 07.54	18.824	–	–	120	–	–	25	–	–	5.67 ± 0.20
2009 Dec 08.54	19.824	90	70	120	–	–	25	–	–	5.45 ± 0.20
2009 Dec 09.22	20.504	–	90	120	–	–	25	–	–	5.27 ± 0.07
2010 Apr 10.97	143.254	–	–	–	250	275	50	9.24 ± 0.15	7.74 ± 0.15	5.45 ± 0.20
2010 Apr 11.97	144.254	120	120	80	–	–	–	–	–	–
2010 Apr 21.94	154.224	300	200	200	–	–	–	–	–	–
2010 Apr 22.94	155.224	120	80	60	–	–	–	–	–	–
2010 Apr 23.93	156.214	120	80	60	–	–	–	–	–	–
2010 Apr 29.92	162.204	150	100	100	–	–	–	–	–	–
2010 Apr 30.92	163.204	300	–	–	625	550	50	9.50 ± 0.09	7.99 ± 0.09	6.57 ± 0.10
2011 Apr 15.95	513.234	–	–	–	1000	500	105	12.82 ± 0.15	13.03 ± 0.15	12.46 ± 0.20
2011 Apr 22.96	520.244	–	–	–	1000	750	105	13.55 ± 0.12	13.28 ± 0.10	12.32 ± 0.12

Table 2. Log of the optical photometric observations of V496 Sct. The date of optical maximum is taken to be 2009 November 18.716 UT.

Date (UT)	Days since optical maximum	V	$B-V$	$V-R_c$	$V-I_c$
2009					
Nov 10.692	−8.024	8.341	0.647	0.471	0.933
Nov 10.710	−8.006	8.329	0.707		
Nov 11.693	−7.023	8.057	0.725	0.506	0.961
Nov 11.705	−7.011	8.009	0.709		
Nov 12.698	−6.018	7.393	0.712		
Nov 12.700	−6.016	7.463	0.680	0.479	0.935
Nov 12.736	−5.980	7.487	0.672	0.469	0.913
Nov 13.732	−4.984	7.585	0.711	0.457	0.914
Nov 17.706	−1.010	7.219	0.772	0.508	1.051
Nov 18.716	0.000	7.070	0.797	0.526	1.037
Nov 19.710	0.994	7.115	0.713	0.472	1.000
Nov 20.699	1.983	7.271	0.708	0.495	1.021
Nov 21.706	2.990	7.554	0.620	0.572	1.144
Nov 23.687	4.971	7.455	0.524	0.567	1.144
Nov 24.687	5.971	7.401	0.545	0.542	1.107
Nov 25.690	6.974	7.473	0.578	0.550	1.101
Nov 28.686	9.970	7.327	0.581	0.549	1.053
Dec 2.681	13.965	7.508	0.583	0.550	1.109
Dec 3.682	14.966	7.907	0.484	0.668	1.212
Dec 14.688	25.972	8.250	0.450	0.759	1.251
Dec 18.692	29.976	8.190			1.097
2010					
Feb 2.221	75.505	9.607	0.351		1.402
Feb 8.212	81.496	9.861	0.301	1.053	1.436
Feb 15.204	88.488	10.373	0.141	1.154	1.561
Feb 27.196	100.480	11.178	0.375	1.477	1.764
Mar 6.163	107.447	11.684	0.501	1.796	2.003
Mar 14.172	115.456	11.143	0.152	1.412	1.588
Mar 16.165	117.449	11.229	0.175	1.500	1.591
Mar 24.168	125.452	11.162	0.320	1.461	1.465
Mar 27.172	128.456	11.314			1.375
Apr 2.141	134.425	11.306	0.297	1.412	1.259
Apr 7.119	139.403	11.327	0.288	1.409	1.244
Apr 15.110	147.394	11.405	0.290	1.417	1.182
Apr 20.128	152.412	11.466	0.290	1.375	1.127
Apr 28.094	160.378	11.439	0.292	1.313	1.037
May. 17.020	179.305	11.411	0.315	1.117	0.823
May. 18.089	180.374	11.377	0.387	1.074	0.794
May. 19.067	181.352	11.401	0.352	1.087	0.770
May. 21.040	183.324	11.371	0.376	1.005	0.742
May. 25.004	187.289	11.424	0.310	1.090	0.740
May. 28.008	190.293	11.395	0.386	0.994	0.678
Jun 4.004	197.289	11.413	0.359	0.920	0.653
Jun 10.978	204.262	11.447	0.381	0.877	0.557
Jun 21.950	215.235	11.448	0.516	0.711	0.416
Jun 28.918	222.202	11.607	0.293	0.816	0.464
Jul 8.947	232.232	11.584	0.501	0.641	0.315
Jul 16.906	240.191	11.680	0.455	0.657	0.268
Jul 24.914	248.199	11.677	0.602	0.514	0.170
Aug 1.962	256.246	11.770	0.559	0.513	0.171
Aug 16.905	271.189	11.841	0.666	0.396	0.052
Aug 22.883	277.167	11.925	0.627	0.404	0.012
Aug 31.866	286.150	11.937	0.759	0.302	−0.044
Sep 10.859	296.080	11.999	0.796	0.238	−0.111
Sep 20.774	305.995	12.085	0.772	0.212	−0.136
Sep 29.844	315.065	12.141	0.774	0.193	−0.139
Oct 10.752	325.973	12.188	0.843	0.139	−0.211
Oct 19.777	334.998	12.225	0.878	0.098	−0.230
Oct 27.762	342.984	12.267	0.915	0.097	−0.220
Nov 12.744	358.965	12.387			

Table 2 – *continued*

Date (UT)	Days since optical maximum	V	$B-V$	$V-R_c$	$V-I_c$
2011					
Feb 10.212	448.433	12.773			−0.557
Feb 23.190	461.411	12.813	1.040	−0.234	−0.642
Mar 20.151	486.372	12.933	1.066	−0.287	−0.624
Apr 13.141	511.362	13.029			−0.858
Apr 18.087	516.308	13.128	0.901	−0.187	−0.683
Apr 21.088	519.309	13.109	0.957	−0.256	−0.672

Table 3. Log of the Varese optical spectroscopy of V496 Sct. The date of optical maximum is taken as 2009 November 18.716 UT.

Date	UT	Expt (s)	Disp (Å pixel^{-1})	λ range (Å)	Days since optical maximum
2009 Nov 9	18:26	1500	2.12	3960–8600	−8.955
10	18:15	3600	Echelle	3950–8640	−7.960
12	17:06	900	2.12	3955–8595	−6.005
12	17:50	1800	Echelle	3880–8640	−5.987
19	16:52	360	2.12	3955–8590	0.972
19	17:57	3600	Echelle	3950–8650	1.016
21	16:53	420	2.12	3965–8610	2.973
21	17:54	3600	Echelle	4180–8650	3.015
24	17:46	2700	Echelle	3955–8645	6.012
28	17:07	2700	Echelle	4020–8655	9.995
Dec 1	17:23	900	Echelle	3955–8645	13.002
1	17:58	900	2.12	3945–8590	13.017
5	17:09	3600	Echelle	3950–8645	16.996
10	17:04	1800	Echelle	3950–8640	21.994
10	17:34	300	2.12	3945–8597	22.007
2010 Mar 13	04:43	1020	4.24	3800–8385	114.469
Apr 28	02:39	2400	2.12	3965–8600	160.384
Jun 06	01:13	3600	2.12	3975–8615	199.331
Jun 22	23:07	3600	2.12	3975–8600	216.245
Jul 15	23:24	3600	Echelle	3950–8640	239.252
Oct 05	19:16	3600	2.12	3925–8565	321.082
2011 Apr 19	02:47	5400	2.12	4000–8640	516.387

2-arcsec wide slit, oriented along the instantaneous parallactic angle. All spectra (including Echelle ones) were calibrated in absolute fluxes by observations of several spectrophotometric standards each night, at similar airmasses and both immediately before and after the exposure on the nova. Their zero-points were then checked against simultaneous *BVRI* photometry by integrating the band transmission profiles on the fluxed spectra, with the differences almost never exceeding 0.1 mag.

3 RESULTS

3.1 The optical light curve

3.1.1 The pre-maximum rise, outburst luminosity, reddening and distance

The optical light curve based on Table 2 is presented in Fig. 1. There is a good photometric coverage of the nova's rise to the maximum which lasts for almost 10 days culminating in a peak brightness of $V_{max} = 7.07$ on 2009 November 18.716 UT. The early

decline after the maximum was observed till mid-December and subsequently the solar conjunction of V496 Sct resulted in the lack of its observational coverage till early 2010 February. We determine the rate of decline by doing a least-squares regression fit to the post-maximum light curve and estimate t_2 to be 59 ± 5 d. The estimated value of t_2 makes V496 Sct as one of the moderately fast Fe II class of novae in recent years. V496 Sct is one of the large amplitude novae observed in recent years with $\triangle R \geq 13.5$ mag (Guido & Sostero 2009). These observed values of the amplitude and t_2 for V496 Sct put it close to the upper limit in the observed spread of the amplitude versus decline rate plot for classical novae presented by Warner (2008, fig. 2.3). Using the maximum magnitude versus rate of decline (MMRD) relation of della Valle & Livio (1995), we determine the absolute magnitude of the nova to be $M_V = -7.0 \pm 0.2$. The reddening is derived using the intrinsic colours of novae at peak brightness, namely $(B - V) = 0.23 \pm 0.06$, as derived by van den Bergh & Younger (1987). We have used our optical photometry data to calculate $E(B - V)$. The observed $(B - V) = 0.797 \pm 0.014$ results in $E(B - V) = 0.57 \pm 0.06$. We have also estimated $E(B - V)$ using the interstellar lines and diffuse interstellar band (DIB) registered in our high-resolution optical spectra. The Na I line is composed of at least five independent components, of which three are well isolated and the remaining two are blended. Following Munari & Zwitter (1997), we estimate a total value of $E(B - V) = 0.65$ from these five components. The interstellar line of K I, though underexposed in the observed spectra, gives a value of $E(B - V) \sim 0.60$ and the DIB λ6614 gives $E(B - V) = 0.65$. These estimates of interstellar reddening are in good agreement with each other, and in the rest of this paper we adopt $E(B - V) = 0.57 \pm 0.06$ and $A_V = 1.77 \pm 0.06$ for a standard reddening law $R = 3.1$. In their study of the spatial distribution of the interstellar extinction, Neckel & Klare (1980) have shown that close to the direction of V496 Sct, A_V shows a value of $\sim$1.8 mag around 3 kpc and a moderate value of A_V estimated by us appears reasonable. By using the MMRD relation of della Valle & Livio (1995) and taking the value of $E(B-V) = 0.57 \pm 0.06$, we obtain the distance $d = 2.9 \pm 0.3$ kpc to the nova. By using the relations for the blackbody angular diameter and temperature, the expansion rate for the ejecta and the distance to the nova given by Ney & Hatfield (1978) and Gehrz (2008), respectively, we estimate a value $\sim$9 kpc for the distance to the nova. This value is more than three times the value estimated by the MMRD relation of della Valle & Livio (1995). A likely reason for this discrepancy is the behaviour of the pseudo-photosphere as a grey-body with reduced emissivity in the fireball phase as seen earlier in the case of V1280 Sco (Das et al. 2008) and V5579 Sgr (Raj, Ashok & Banerjee 2011).

3.1.2 The nature of the light curve

A classification system for the optical light curves for novae, based on a large sample of American Association of Variable Star Observers (AAVSO), has been presented by Strope, Schaefer & Henden (2010). Their classification system defines seven classes based on the time to decline by 3 mag from the peak, t_3, and the shape of the light curve. The shape of the optical light curves of V496 Sct presented in Fig. 1 has all the characteristics of D class of nova. The early decline following the rise to the maximum is interrupted by a fast decline around 90 days after the outburst reaching the minimum brightness close to 120 days near the centre of the dust dip. The brightness has been recovered to a value below the original decline. Thus, the classification of the optical light curve for V496 Sct is D(90), as the estimated value of t_3 is $\sim$90 days for V496 Sct.

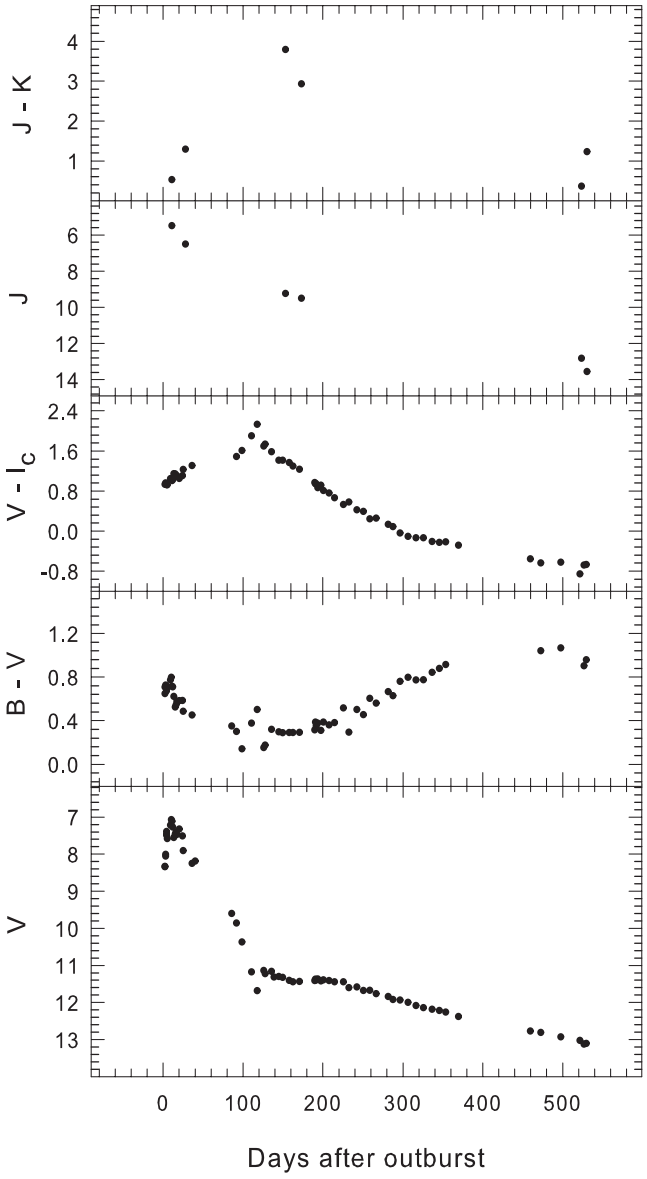

Figure 1. The light curve of V496 Sct from Asiago and Mt. Abu data.

3.2 Line identification, evolution and general characteristics of the *JHK* spectra

The *JHK* spectra are presented in Figs 2–4, respectively; the observed line list is given in Table 4. The IR observations presented here cover all the phases with the first *J*-band spectrum taken on 2009 November 19 very close to the visual maximum. This *J*-band spectrum is dominated by the lines of H I, N I, C I and O I all displaying deep P Cygni profiles. The FWHM of the emission and the absorption components of the Pβ line are 700 and 270 km s^{-1}, respectively. The absorption component is blueshifted by 960 km s^{-1} from the emission component. The next set of spectra taken at the beginning on 2009 December 3 shows the disappearance of P Cygni profiles and predominant emission components for all the lines. The typical FWHM of the H I lines is 1230 ± 50 km s^{-1}. The ratio of the observed strength of the O I lines, $W(1.1287)/W(1.3164) \sim 3$,

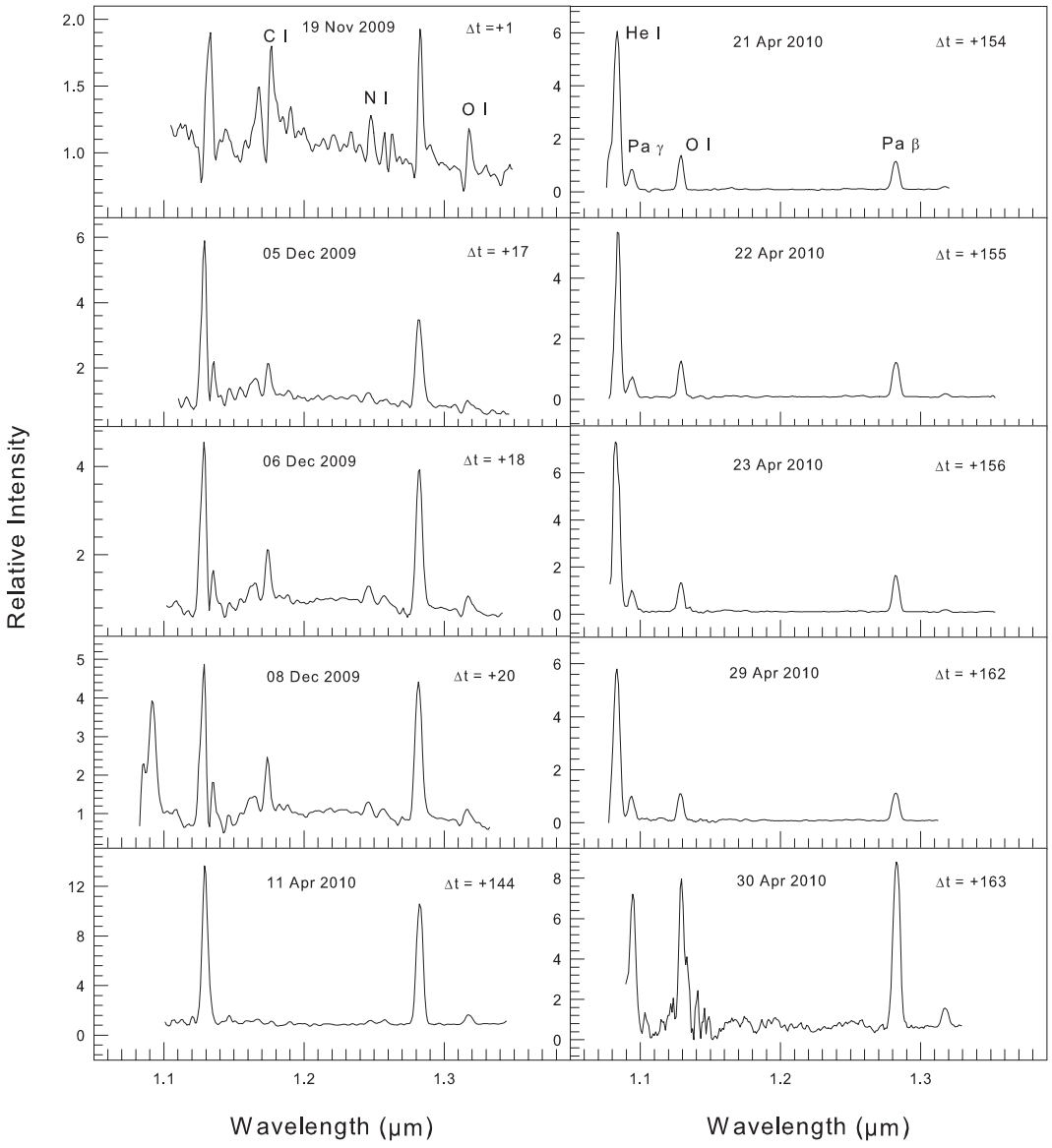

Figure 2. The *J*-band spectra of V496 Sct are shown at different epochs. The relative intensity is normalized to unity at 1.25 μm. The time from optical maximum is given for each spectrum.

indicates that Lyβ fluorescence is the dominating pumping mechanism and this is corroborated by the strong O I λ8446 line seen in the optical spectra discussed later. A noticeable feature of these early spectra is the presence of lines due to Na I and Mg I. In the spectra taken on 2009 December 5, the Na I lines at 1.1404, 2.1452, 2.2056 and 2.2084 μm and Mg I lines at 1.1828, 1.5040, 1.5749 and 1.7109 μm are clearly seen. In an earlier study of V1280 Sco, Das et al. (2008) had suggested that the presence of spectral lines of low ionization species like Na I and Mg I in the early spectra are indicators of low-temperature zones conducive to dust formation in the nova ejecta and this is very well borne out in the case of V496 Sct. We would like to point out the presence of a large number of strong lines of neutral carbon seen in the *JHK* bands. These are typical of the Fe II type nova as seen in the case of V2615 Oph (Das, Banerjee & Ashok 2009) and V5579 Sgr (Raj et al. 2011).

The most interesting spectral features seen in the spectra of V496 Sct taken in 2009 December are the prominent first overtone CO bands in the *K* band and they are discussed in Section 3.3. The last spectra, before V496 Sct became inaccessible due to its conjunction with the Sun, was taken on 2009 December 9.

The set of spectra taken in 2010 April, after V496 Sct emerged from its solar conjunction, shows strong He I lines at 1.0830 μm in the *J* band and 2.0581 μm in the *K* band. The He I 1.0830-μm line exceeds in strength compared to H I lines indicating higher excitation conditions in the nova ejecta. The other weaker He I lines at 1.7002 and 2.1120–2.1132 μm are also seen. The rising continuum seen in the spectra taken on 2010 April 11 indicates that the dust detected by Russell et al. (2010) on 2010 February 10 is still present.

3.3 Modelling and evolution of the CO emission

We adopt the model developed in our earlier work on V2615 Oph (Das et al. 2009) to characterize the CO emission. Briefly, in this model the CO gas is considered to be in thermal equilibrium with the

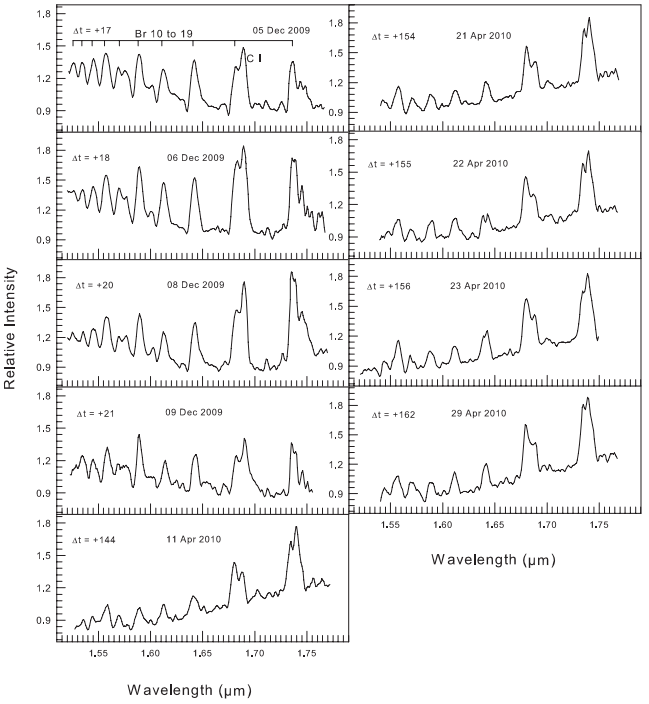

Figure 3. The *H*-band spectra of V496 Sct are shown at different epochs. The relative intensity is normalized to unity at 1.65 μm. The time from optical maximum is given for each spectrum.

same temperature for calculating the level populations of rotation and vibration bands. It is assumed that the rotational levels are Gaussian in shape. In addition to ^{12}C ^{16}O the other isotopic species included in the calculations is ^{13}C ^{16}O. The isotopic species like ^{12}C ^{17}O and ^{12}C ^{18}O are not considered as they are expected to have low abundances. The model luminosity E which is in units of erg s^{-1} is converted to erg cm^{-2} s^{-1} μm^{-1} by dividing with $4\pi d^2$, where d is the distance to the source and scaling to a unit wavelength. The peak intensities of the vibration bands are analytically determined such that the integrated area under the curve matches the expected observed quantity $E/4\pi d^2$. An appropriate continuum determined from the *K*-band photometry for a particular date is added to the model CO emission so that it can be compared with the observed CO emission bands. The input parameters to the model are the total mass of the CO gas ($M_{\rm CO}$), the ^{12}C/^{13}C ratio denoted as a constant α and the gas temperature $T_{\rm CO}$. For a given set of values for $M_{\rm CO}$, α, $T_{\rm CO}$ and d, the CO flux estimated from the model is an absolute quantity. The representative model spectra matching the observed data for 2009 December 5 and 7 are shown in Fig. 5.

The best-fitting model spectra to the observed data are obtained by varying the input parameters $M_{\rm CO}$, α and $T_{\rm CO}$. The expected changes to the model spectra by varying these input parameters may qualitatively be summarized as follows. The increase in $M_{\rm CO}$ enhances the absolute level of the CO emission, while the increase in $T_{\rm CO}$ changes the relative intensities of different vibrational bands in addition to changing the absolute level of the emission. The CO emission is assumed to be optically thin. The C I lines at 2.2906 and 2.3130 μm and Na I lines at 2.3348 and 2.3379 μm are also likely to be present in the spectral region covered by the CO emission giving rise to some deviations between the best model fit and the observed spectra. In addition, since a comparison of the relative strengths of the vibrational bands within the first overtone allows the gas temperature to be determined, we are handicapped by being able to detect only three of the bands (v = 2–0, 3–1, 4–2). Within these constraints, our formal model fits for 2009 December 5 and 7 yield temperatures of 4000 ± 500 and 3600 ± 500 K, respectively, with a reasonably similar range in mass of $M_{\rm CO} = 1.5$–2×10^{-8} M$_\odot$. The representative fits for 2009 December 5 and 7 are shown in Fig. 5. The model calculations also show that the $v = 2-0$ bandhead of ^{13}CO at 2.3130 μm becomes discernibly prominent if the ^{12}C/^{13}C ratio is $\leq$1.5. As this spectral feature is not clearly detected in our observed spectra, we place a lower limit of $\sim$1.5 for the ^{12}C/^{13}C ratio. However, we add a cautionary note that the signal-to-noise ratio (S/N) in the region of ^{12}CO and ^{13}CO bands is about 15–20 and better quality spectra may permit a more accurate determination of the CO gas parameters. The lower limit of $\sim$1.5 for the ^{12}C/^{13}C ratio reported here is the lowest value till date among the novae that have displayed the first overtone bands of CO.

It may be helpful to compare the observed ^{12}C/^{13}C ratio in V496 Sct with the values for other novae that have displayed the first overtone bands of CO and also the model-predicted values. The observed values for the ^{12}C/^{13}C ratio available in the literature are $\geq$5 in V705 Cas (Evans et al. 1996), $\geq$3 in NQ Vul (Ferland et al. 1979), $\geq$2 in V2615 Oph (Das et al. 2009), $\simeq$2.9 in V842 Cen (Wichmann et al. 1991) and $\simeq$1.2 in V2274 Cyg (Rudy et al. 2003). The thermonuclear runaway (TNR) responsible for the nova outburst is one of the important sources for the production of ^{13}C isotopes (Starrfield et al. 1972; Starrfield, Sparks & Truran 1974; Romano & Matteucci 2003). Hajduk et al. (2005) have pointed out that the outburst of born-again giants like V4334 Sgr are another source for ^{13}C isotopes in the Galaxy; a low value for the ratio ^{12}C/^{13}C = 5 was observed by Pavlenko et al. (2004) in V4334 Sgr. In the hydrodynamical models of nova outbursts, the ^{12}C/^{13}C ratio will depend on parameters like the mass of the underlying white dwarf, the accretion history and mixing of the accreted material from the companion star with the surface material of the white dwarf (Starrfield, Gehrz & Truran 1997; Jose & Hernanz 1998; Yaron et al. 2005). The estimated lower limits as well as the observed values for ^{12}C/^{13}C ratio in the case of novae discussed about indicate that ^{13}C is possibly not synthesized at the high values predicted by these theoretical models. In the novae mentioned above that displayed CO bands, the estimated $M_{\rm CO}$ ranges from 2.8×10^{-10} M$_\odot$ (V705 Cas) to 3×10^{-8} M$_\odot$ (V2615 Oph). The present value of $M_{\rm CO} = 1.5$–2×10^{-8} M$_\odot$ for V496 Sct lies within this range and is similar to the CO mass determined in V2615 Oph.

3.4 Line identification, evolution and general characteristics of the optical spectra

The optical spectra presented here cover the pre-maximum rise, the optical maximum brightness, the early decline and the nebular phase. There are very few novae for which the spectral evolution before the maximum brightness has been documented, e.g. V1280 Sco (Kuncarayakti, Kristyowati & Kunjaya 2008; Naito et al. 2012) and V2615 Oph (Munari et al. 2008a). The spectral evolution of V496 Sct during the pre-maximum, maximum and optically thick branch of the decline phase is presented in Fig. 6, while the subsequent evolution during the optically thin and nebular phase is covered in Fig. 7. Fig. 8 documents the complex evolution of profiles of the Fe II λ5018 line and Fig. 9 documents the temporal evolution of the velocity of the absorption components of the Fe II λ5018 line. A summary of emission lines identified in the optical spectra is provided in Table 5, and dereddened fluxes (according to $E_{B-V} = 0.57$ and an $R_V = 3.1$ reddening law) of the prominent emission lines relative to Hβ are given in Table 6 for some representative dates.

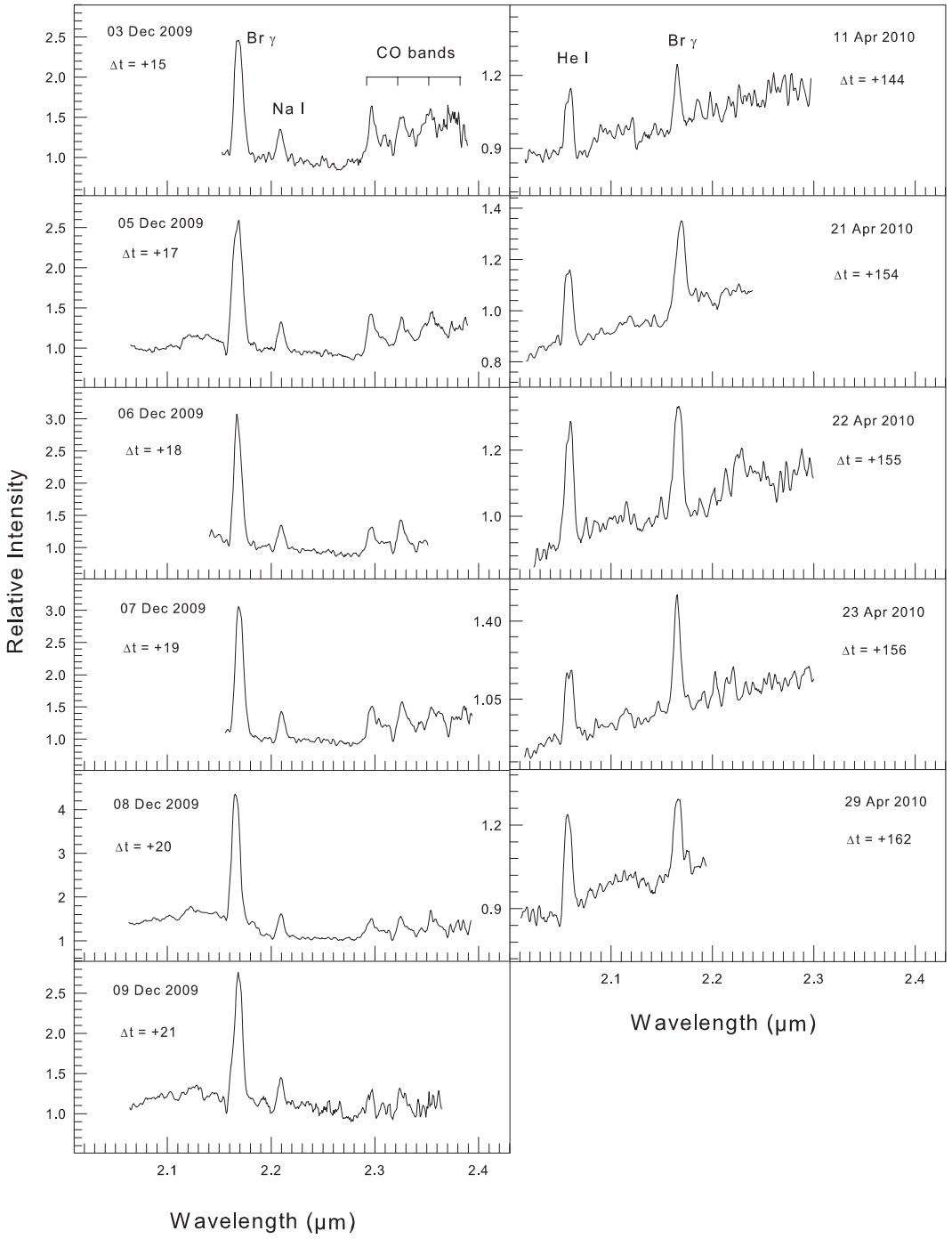

Figure 4. The *K*-band spectra of V496 Sct are shown at different epochs. The relative intensity is normalized to unity at 2.2 μm. The time from optical maximum is given for each spectrum.

3.4.1 Pre-maximum rise and optical maximum

There is considerable interest in studying the spectral evolution during the pre-maximum rising phase of classical novae, an evolutionary phase rarely observed. The pre-maximum spectra of V496 Sct in Fig. 6 are characterized by emission lines confined to just Fe II (multiplets 27, 28, 37, 38, 42, 48, 49, 55 and 74) and hydrogen Balmer series, with feeble O I λ7772, 8446.

During the rise towards maximum the barycentric and terminal velocity of P Cygni absorptions, and the FWHM of both absorption and emission components declined with time (see Fig. 6). The terminal and core velocity of the P Cygni absorption component of Hα line in Fig. 6 declined from -2000 and -700 km s^{-1} on day -9 to -1200 and -600 km s^{-1} on day -6, while at the same time the FWHM of the absorption and emission components declined from 1000 to 700 km s^{-1}. The P Cygni components essentially vanished at the time of maximum brightness. When they reappeared later into early decline they were much sharper (FWHM = 250 km s^{-1}) and blueshifted (core velocity = -1350 km s^{-1}) than at pre-maximum.

The high-resolution Echelle spectra listed in Table 3 show that the broad and single P Cygni absorption components observed on

Table 4. A list of the lines identified from the *JHK* spectra. The additional lines contributing to the identified lines are listed.

Wavelength (μm)	Species	Other contributing lines and remarks
1.0830	He I	
1.0938	Pa γ	
1.1287	O I	
1.1404	Na I	C I 1.1415
1.1600–1.1674	C I	Strongest lines at 1.1653, 1.1659,1.16696
1.6872	Fe II	
1.1746–1.1800	C I	Strongest lines at 1.1748, 1.1753,1.1755
1.1828	Mg I	
1.1880	C I	
1.2074	N I	
1.2187, 1.2204	N I	
1.2249, 1.2264	C I	
1.2329	N I	
1.2382	N I	
1.2461, 1.2469	N I	Blended with O I 1.2464
1.2562, 1.2569	C I	Blended with O I 1. 2570
1.2818	Pa β	
1.2950	C I	
1.3164	O I	
1.5040	Mg I	Blended with Mg I 1.5025, 1.5048
1.5256	Br 19	
1.5341	Br 18	
1.5439	Br 17	
1.5557	Br 16	
1.5701	Br 15	
1.5749	Mg I	Blended with Mg I 1.5741, 1.5766, C I 1.5788
1.5881	Br 14	Blended with C I 1.5853
1.6005	C I	
1.6109	Br 13	
1.6407	Br 12	
1.6806	Br 11	
1.6890	C I	
1.7002	He I	
1.7045	C I	
1.7109	Mg I	
1.7234–1.7275	C I	Several C I lines
1.7362	Br 10	Affected by C I 1.7339 line
1.7449	C I	
1.7605–1.7638	C I	
2.0581	He I	
2.1120, 2.1132	He I	
2.1156–2.1295	C I	
2.1452	Na I	
2.1655	Br γ	
2.2056, 2.2084	Na I	
2.2156–2.2167	C I	
2.29–2.40	CO	$\Delta v = 2$ bands
2.2906	C I	
2.3130	C I	

2009 November 10 and 12 of H I and Fe II multiplets are replaced by two narrow components on 2009 November 19. The two absorption components in the case of Fe II λ5018, shown in Fig. 8, are located at heliocentric velocities of −785 and −360 km s^{-1}.

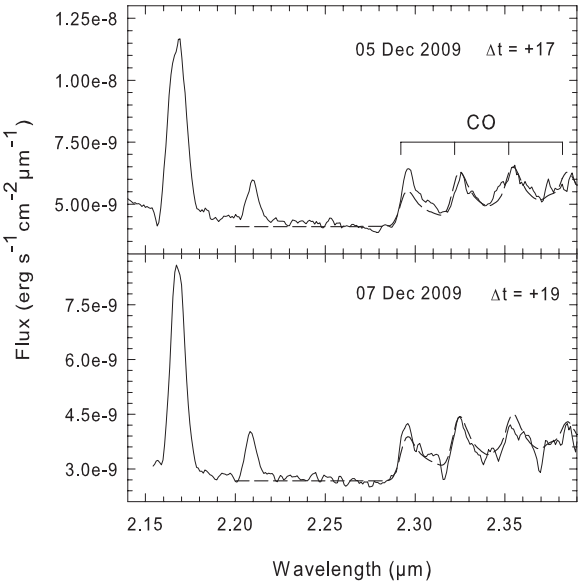

Figure 5. The model fits are shown as dashed lines to the observed first overtone CO bands in V496 Sct for 2009 December 5 and 7. The fits are made for a constant CO mass of 2e−8 $M_\odot$ on both the days while the temperature of the gas T_{CO} is 4000 and 3600 K, respectively. The time from optical maximum is given for each spectrum.

3.4.2 Absorption systems during early decline

The Echelle spectra offer the possibility to observe at high resolution the evolution of the absorption components. As illustrated in Fig. 8, when the nova reached its maximum brightness, the broad and single absorption components of P Cygni line profile were replaced by two components, whose intensity gradually faded in parallel with the decline in brightness of the nova. A similar behaviour was exhibited by V2615 Oph where two absorption components are seen in addition to the emission component following the optical maximum (Munari et al. 2008a). Fig. 8 presents line profiles for Fe II λ5018 from the high-resolution Echelle spectra to illustrate the evolution of the two absorption components. Both absorption components increased their negative radial velocity with time, with a linear trend as illustrated in Fig. 9 and the best-fitting lines are given by the following expressions:

$$V_A = -343 - (9.2 \times t), \quad (1)$$

$$V_B = -763 - (18.5 \times t), \quad (2)$$

where t is the time after the optical maximum. The approaching conjunction with the Sun prevented further observations of V496 Sct after our 2009 December 10, 22 days past the optical maximum, and the next set of observations was resumed from 2010 March 13. Novae usually display different absorption systems, which behave similarly from object to object, and that have been studied in detail by McLaughlin (1960, hereafter McL60), who introduced a handy nomenclature for them. An impressive graphical representation of them has been offered by Hack & Struve (1970, fig. 4i) from very high resolution observation of Nova Del 1967 by Ch. Fehrenbach. The A and B components of equations (1) and (2) shown in Fig. 9 nicely correspond to the principal and diffuse enhanced absorption systems described by McL60, who noted a clear correlation between the t_2, t_3 decline times and the mean velocity of these absorption systems. McL60 also noted how the radial velocities of these

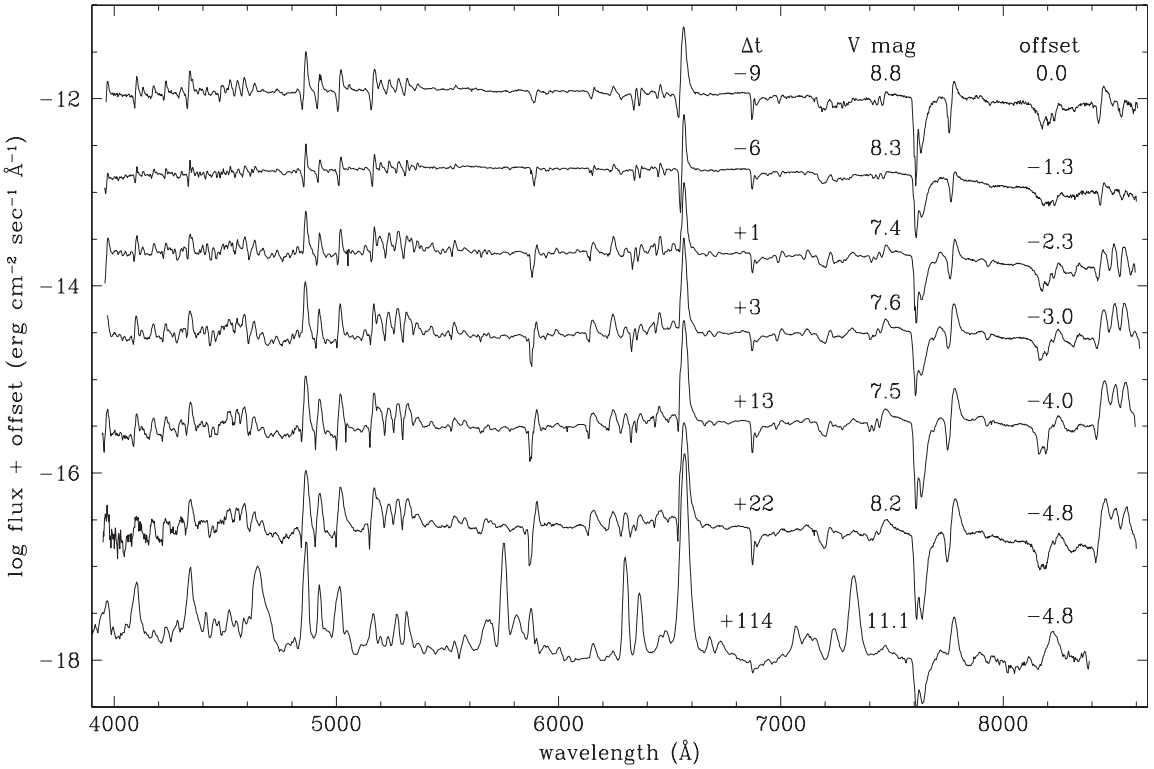

Figure 6. Low-resolution spectroscopic evolution of V496 Sct from pre-maximum to the end of the optically thick branch (pre-nebular stage) of the light curve. For the first month of the evolution the emission lines are mostly due to Fe II and H I, with also O I λλ7772, 8446, Na I λ5893 and Ca II λλ8498, 8542. The last spectrum is plotted for commonality also in Fig. 7. The time from optical maximum, the *V*-band magnitude and the offset in log flux are given for each spectrum.

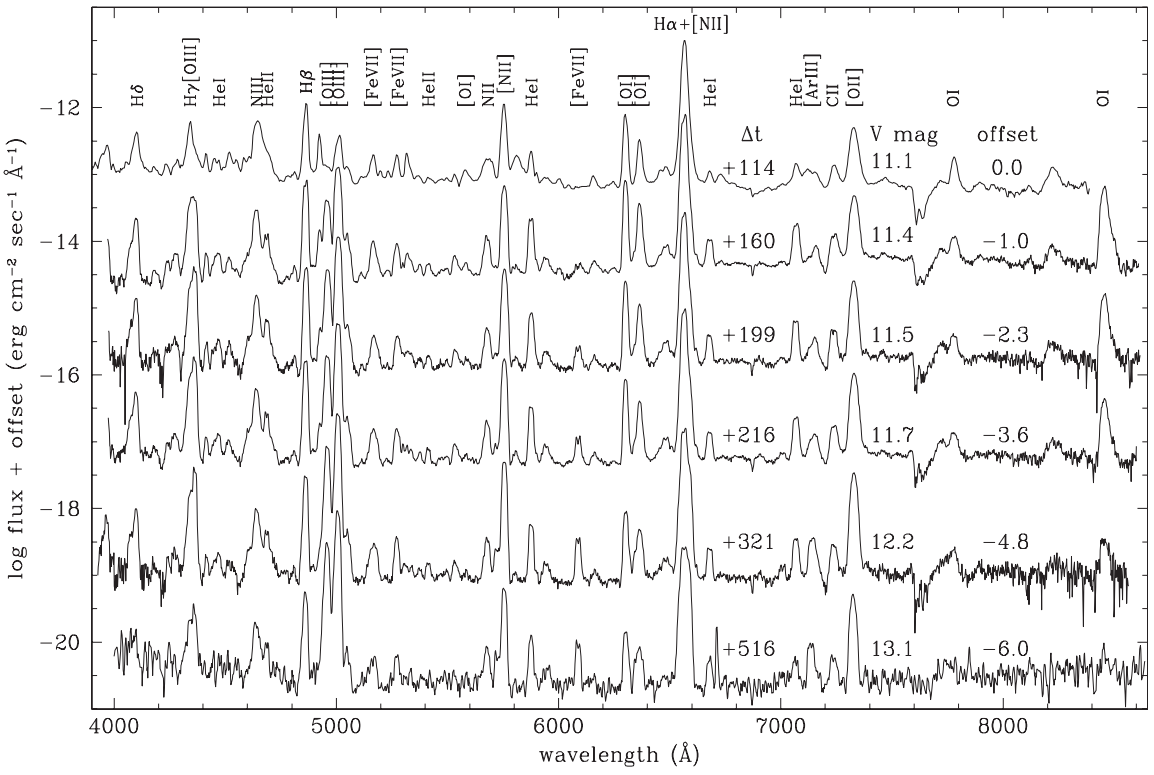

Figure 7. Low-resolution spectroscopic evolution of V496 Sct during the optically thin branch (nebular condition) of the light curve, with time from optical maximum, the *V*-band magnitude and the offset in log flux are given for each spectrum. The major emission lines are identified.

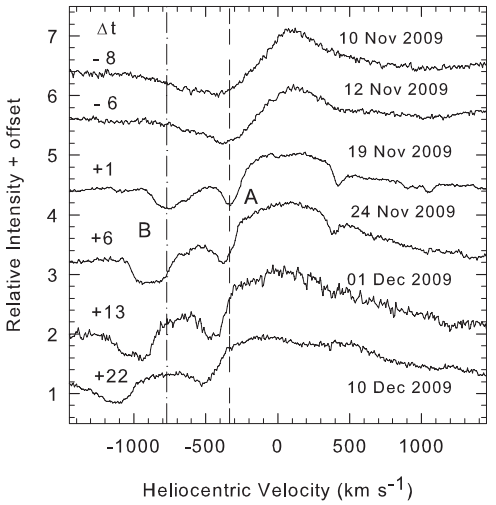

Figure 8. Profiles of the Fe II λ5018 line in the pre-maximum rise, near optical maximum and the early decline phases. The initial positions of the two narrow absorption components are shown by the broken lines. The time from optical maximum is given for each spectrum.

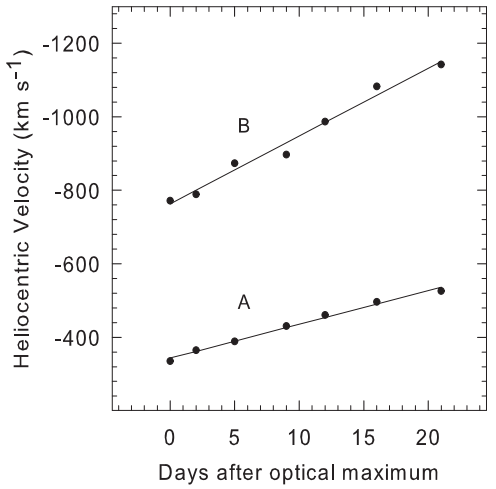

Figure 9. The time evolution of radial velocities of the two absorption components of the Fe II λ5018 line.

absorption systems generally increase with time, as seen here in V496 Sct.

The McL60 velocity relation for the principal system is $\log v_{\rm prin} = 3.57 - 0.5 \log t_2$, and predicts a mean of $-485\,{\rm km\,s^{-1}}$ for the $t_2 = 59$ d of V 496 Sct. The agreement with Fig. 9 is evident, considering in particular that the approaching conjunction with the Sun prevented to extend the observations to later epoch characterized by larger radial velocities for both systems. The McL60 velocity relation for the diffuse enhanced system is $\log v_{\rm diff-enh} = 3.71 - 0.4 \log t_2$, and it predicts $-1005\,{\rm km\,s^{-1}}$ for the $t_2 = 59$ d of V496 Sct, again in good agreement with Fig. 9. Munari et al. (2008a) have pointed out similar agreement of the observed velocities for the absorption systems of Hα in the case of V2615 Oph with the predicted values using the statistical relations by McL60.

For a few days around the optical maximum, the high-resolution spectra displayed a rich ensemble of very sharp absorption lines of modest radial velocity displacement, due to low ionization metals like Ti II, which will be investigated elsewhere. They are similar to the transient heavy element absorption systems resulting from the

Table 5. A list of the prominent emission lines identified from the optical spectra.

Wavelength (Å)	Species
3970	Ca II and Hϵ
4101	Hδ
4129	Fe II(27)
4173	Fe II(27)
4233	Fe II(27)
4303	Fe II(27)
4340	Hγ
4351	Fe II(27)
4363	[O III]
4555	Fe II(37)
4586	Fe II(38)
4634	N III
4649	O II
4686	He II
4861	Hβ
4924	Fe II(42)
4959	[O III]
5007	[O III]
5018	Fe II(42)
5046	Si II
5159	[Fe VI] + [Fe VII]
5169	Fe II + Mg I
5235	Fe II(49)
5270	[Fe III]
5276	Fe II(49+48)
5309	[Ca V]
5316	Fe II(49)
5361	Fe II(48)
5415	He II
5535	Fe II(55) + N II
5676	N II
5755	[N II](3)
5876	He I
5890	Na I
5909	Fe II
5942	N II(28)
5991	Fe II(46)
6086	[Ca V] + [Fe VII]
6084	Fe II(46)
6157	O I
6243	Fe II + N II
6300	[O I]
6347	Si II(2)
6363	[O I]
6419	Fe II(74)
6431	Fe II(40)
6456	Fe II
6563	Hα
6678	He I
6726	O I(2)
7065	He I
7139	[Ar III]
7234	C II(3, blend of 7231 and 7236)
7330	[O II]
7774	O I
8446	O I
8498	Ca II triplet
8542	Ca II triplet

Table 6. Fluxes of prominent emission lines relative to Hβ = 100. The fluxes of the emission lines including Hβ are corrected for $E(B-V) = 0.57$.

Wavelength (Å)	Species	2009 Nov 09	2009 Nov 19	2009 Dec 10	2010 Apr 28
3970	Ca II and Hϵ	28.3	39.4	30.0	
4101	Hδ	45.2	36.6	7.2	54.2
4173	Fe II(27)	27.7	24.7	18.0	
4340	Hγ	21.1	11.8	36.2	141.5
4584	Fe II(38)	48.2	37.3	19.8	
4635	N III	13.3	42.9	14.2	41.5
4686	He II				9.3
4861	Hβ	100	100	100	100
4924	Fe II(42)	31.3	44.7	39.8	5.9
4959	[O III]				48.3
5007	[O III]				182.2
5018	Fe II	36.8	35.0	58.5	
5169+5176	Fe II + Mg I + N II	36.8	21.7	64.2	11.0
5535	Fe II(55) + N II	3.6	8.1	6.1	
5577	O I			3.7	
5675	N II				10.2
5755	[N II](3)				66.1
5876	He I				22.0
5890	Na I		10.5	11.4	
6157	O I	2.4	10.7	10.6	
6243	Fe II + N II	12.7	29.0	14.0	
6300	[O I]			12.3	58.5
6363	[O I]			6.8	28.0
6456	Fe II	6.0	19.9	11.8	
6563	Hα	234.9	195.7	240.3	690.7 [a]
6678	He I				8.5
7065	He I				15.3
7330	[O II]				44.9
7774	O I	18.1	12.5	19.1	5.1
8446	O I	6.0	14.2	16.9	47.5
8498	Ca II triplet		20.3	5.4	
8542	Ca II triplet		16.6	9.1	
Hα/Hβ		2.4	2.0	2.4	6.9
Hβ	10^{-11} erg cm^{-2} s^{-1}	16.6	71.8	97.0	11.8

[a][N II] $\lambda\lambda$6548, 6584 expected to contribute significantly to the overall flux of Hα blend.

episodic mass ejection from the secondary star seen in novae by Williams et al. (2008).

The permitted lines of Fe II are the strongest non-Balmer lines both during the pre-maximum rise, near optical maximum and early decline indicating $P_{\rm fe}$ spectral class for V496 Sct during these phases (Williams et al. 1991; Williams, Phillips & Hamuy 1994).

3.4.3 Nebular phase

The spectral evolution during the optically thin branch (nebular phase) is shown in Fig. 7. The evolution has been pretty standard, with [O III] $\lambda\lambda$4363, 4959, 5007, [N II] $\lambda\lambda$5755, 6548, 6584, [O II] λ7325 and [O I] $\lambda\lambda$6300, 6364 being the dominant lines. The [O I] λ6300/λ6364 flux ratio, which was close to 1 during the early phases and indicative of a large optical depth in the lines, with the thinning of the ejecta, the opacity increased towards the 3.1 normal ratio. The Lyβ fluorescent O I λ8446 line has remained strong throughout the outburst and begun declining around day +200 when the optical thinning of ejecta reduced the trapping of Lyβ photons and therefore the fluorescent pumping of O I atoms. The ionization conditions have been steadily increasing with advancing decline, with He I, He II and [Fe VII] lines monotonically increasing in intensity with respect to the other lines. The presence of a feeble [Fe X] λ6375 component could be compatible with the profile for the [O I] λ6360 + [S II] $\lambda\lambda$6347, 6371 blend of the day +516 spectrum in Fig. 7, a firmer conclusion requiring a spectrum of higher S/N and resolution. The spectra shown in Fig. 7 show how the transition of V496 Sct from *permitted* to *nebular* phase occurred at an intermediate time after the last permitted spectrum of 2010 March 13 and the first nebular spectrum of 2010 April 28 where [O III] $\lambda\lambda$4959, 5007 doublet lines are seen prominently. We assign $A_{\rm o}$ spectral class for V496 Sct (Williams et al. 1991, 1994).

The presence of an emission feature at λ4924 coinciding with Fe II(42) line in the spectra taken during 2010 March till June is little puzzling. As the other prominent Fe II $\lambda\lambda$4584, 5018 lines are absent as expected in the nebular phase, this feature is unlikely to be associated with the Fe II multiplet. We would like to point out the presence of the emission feature at λ4924 as an unidentified feature similar to several such features seen in the spectra of many novae.

3.5 Physical parameters

The emission line fluxes of hydrogen and other elements can be used to estimate the physical parameters of the nova ejecta. In the

early decline phase when the electron number densities are large, it is necessary to take into account the optical depth τ while deriving the physical parameters. We determine the optical depth for the [O I] λ6300 line using the formulation of Williams (1994), viz.,

$$\frac{j_{6300}}{j_{6364}} = \frac{1 - e^{-\tau}}{1 - e^{-\tau/3}}, \quad (3)$$

where j is the line emissivity. For the period from 2010 April 28 to October 5, we get τ in the range of 0.54–3.21. Now from the optical depth and the electron temperature, we can estimate the mass of oxygen in the ejecta using the λ6300 line:

$$M_{\rm O\,I} = 152 d^2 e^{22\,850/T_e} \times 10^{1.05E(B-V)} \frac{\tau}{1 - e^{-\tau}} F\, M_\odot, \quad (4)$$

where F is the flux of λ6300 line. Taking a typical value of $T_e = 5000$ K for the electron temperature (Ederoclite et al. 2006), we find $M_{\rm O\,I}$ in the range 1.18×10^{-5} to 2.28×10^{-6} $M_\odot$. The electron number density N_e can be determined by [O III] line as given in Osterbrock (1989):

$$\frac{j_{4959} + j_{5007}}{j_{4363}} = 7.73 \times \frac{e^{3.29\times10^{-4}/T_e}}{1 + 4.5 \times 10^{-4} \frac{N_e}{T_e^{1/2}}}. \quad (5)$$

The values we obtained are in the range 10^4–10^6 cm^{-3} close to the lower limit of the critical densities to give rise to nebular and auroral lines. This indicates that these lines are arising in relatively low-density regions. Following Osterbrock (1989), we have a relation between the intensity of the Hβ emission line and the mass of hydrogen in the emitting nebula of pure hydrogen as

$$m({\rm H})/M_\odot = \frac{d^2 \times 2.455 \times 10^{-2}}{\alpha^{\rm eff} N_e} I({\rm H}\beta), \quad (6)$$

where $\alpha^{\rm eff}$ is the effective recombination coefficient and I(Hβ) is the flux for Hβ line. The mass of hydrogen m(H) in the ejecta is $(6.3 \pm 0.2) \times 10^{-5}$ $M_\odot$. As noted earlier in Section 3.2, V496 Sct formed dust. The IR observations by Russell et al. (2010) showed the presence of dust on 2010 February 10 which is still present on 2010 April 11 as indicated by the large $(J - K)$ colour and the rising continuum. A sharp decline around 2010 February 8 seen in the V-band light curve presented in Fig. 1 also indicates the onset of dust formation. It would be interesting to make an estimate of the dust mass $M_{\rm dust}$ in V496 Sct and compare it with other novae that formed dust in their ejecta using the thermal component of the spectral energy distribution (SED). We adopt the method described by Woodward et al. (1993) that uses $(\lambda F_\lambda)_{\rm max}$ and $T_{\rm dust}$ values obtained from the thermal component of the SED. It is pertinent to point out that the present *JHK* photometric observations cover mostly the increasing part of the SED and thus the estimate of the temperature for the dust $T_{\rm dust}$ likely to have large uncertainty. We obtain $M_{\rm dust} = 1$–5×10^{-10} $M_\odot$ for 2010 April 30 from the best-fitting value of $T_{\rm dust} = 1500 \pm 200$ K (with χ^2 minimization) for the temperature of the dust shell, $(\lambda F_\lambda)_{\rm max} = 2.62 \times 10^{-16}$ W cm^{-2} and $d = 2.9$ kpc. The estimated masses for different constituents of the ejecta like hydrogen, oxygen and dust derived from the optical and the IR observations may be usefully utilized to derive the gas-to-dust mass ratio in novae. Gehrz et al. (1998) have presented a compilation of $M_{\rm gas}$ and $M_{\rm dust}$ along with the ratio $M_{\rm gas}/M_{\rm dust}$ ranging from 5 in the case of V705 Cas to 3×10^4 in the case of QU Vul. In the case of V2362 Cyg, a very fast Fe II nova, Munari et al. (2008b) have derived a value of 3×10^5 for $M_{\rm gas}/M_{\rm dust}$. Taking the average fractional yield (by mass) of hydrogen to be 0.32 ± 0.10 for white dwarf masses ranging from 0.6 to 1.25 $M_\odot$ as per calculations of Jose & Hernanz (1998) and Starrfield et al. (1997), the total gas mass based on the mass of hydrogen gas (determined here as 6.3×10^{-5} $M_\odot$) is estimated to be $2.0 \pm 0.6 \times 10^{-4}$ $M_\odot$. Hence the gas-to-dust ratio is found to be $M_{\rm gas}/M_{\rm dust} \sim 1.3$–$6.3 \times 10^5$ indicating that a small amount of dust was formed in V496 Sct comparable to 3×10^5 observed in the case of V2362 Cyg by Munari et al. (2008b).

4 SUMMARY

We have presented near-IR and optical spectroscopy and photometry of nova V496 Sct which erupted on 2009 November 8. From the optical light curve, the absolute magnitude and the distance to the nova are estimated to be $M_V = -7.0 \pm 0.2$ and $d = 2.9 \pm 0.3$ kpc, respectively. The IR and optical spectra indicate that the nova is of the Fe II class. Evidence is seen from the *JHK* photometry for the formation of dust in the nova in 2010 April. In this context, the presence of emission lines from low ionization species like Na and Mg in the early spectra and subsequent formation of the dust supports the predictive property of these lines as indicators of dust formation as proposed by Das et al. (2008). V496 Sct is one of the moderately fast Fe II class of novae ($t_2 = 59$ d) that showed CO emission before the dust formation.

The various phases of the spectral evolution of V496 Sct have been identified using the Tololo classification system for novae (Williams et al. 1991, 1994). The permitted lines of Fe II were the strongest non-Balmer lines in the pre-maximum as well as the early decline phase indicating $P_{\rm fe}$ class for the nova. The nova had evolved to the auroral phase $A_{\rm o}$ in 2010 March as the [N II] λ5755 auroral line was the strongest non-Balmer line. We note the absence of [Fe X] λ6375 coronal emission line in the spectra taken as late as 2011 April 19. Thus, the optical spectra show that the nova is evolved in the $P_{\rm fe}A_{\rm o}$ spectral sequence.

ACKNOWLEDGMENTS

The research work at Physical Research Laboratory is funded by the Department of Space, Government of India. We would like to thank A. Frigo, V. Luppi, L. Buzzi, A. Milani, G. Cherini, A. Maitan and L. Baldinelli (ANS Collaboration). We thank the referee for the helpful comments.

REFERENCES

Balam D., Sarty G., 2009, IAU Circ., 9093, 1
Das R. K., Banerjee D. P. K., Ashok N. M., Chesneau O., 2008, MNRAS, 391, 1874
Das R. K., Banerjee D. P. K., Ashok N. M., 2009, MNRAS, 398, 375
della Valle M., Livio M., 1995, ApJ, 452, 704
Ederoclite A. et al., 2006, A&A, 459, 875
Evans A., Geballe T. R., Rawlings J. M. C., Scott A. D., 1996, MNRAS, 282, 1049
Ferland G. J., Lambert D. L., Netzer H., Hall D. N. B., Ridgway S. T., 1979, ApJ, 227, 489
Gehrz R. D., 2008, in Bode M. F., Evans A., eds, Classical Novae. Cambridge Univ. Press, Cambridge, p. 167
Gehrz R. D., Truran J. W., Williams R. E., Starrfield S., 1998, PASP, 110, 3
Guido E., Sostero G., 2009, IAU Circ., 9093, 1
Hack M., Struve O., 1970, Stellar Spectroscopy. Vol. 2: Peculiar Stars, Trieste Oss. Astr., Trieste
Hajduk M. et al., 2005, Sci, 308, 231
Jose J., Hernanz M., 1998, ApJ, 494, 680
Kuncarayakti H., Kristyowati D., Kunjaya C., 2008, Ap&SS, 314, 209
Landolt A. U., 1992, AJ, 104, 340

McLaughlin D. B., 1960, in Greenstein J. L., ed., Stellar Atmospheres. Univ. Chicago Press, Chicago, p. 585 (McL60)
Munari U., Moretti S., 2012, Baltic Astronomy, 21, 22
Munari U., Zwitter T., 1997, A&A, 318, 269
Munari U. et al., 2008a, A&A, 492, 145
Munari U., Henden A., Valentini M., Siviero A., Dallaporta S., Ochner P., Tomasoni S., 2008b, MNRAS, 387, 344
Munari U., Siviero A., Buzzi L., Valisa P., 2009a, IAU Circ., 9093, 1
Munari U., Siviero A., Valisa P., Dallaporta S., Baldinelli L., 2009b, Central Bureau Electronic Telegrams, 2034, 1
Munari U. et al., 2012, Baltic Astronomy, 21, 180
Naito H. et al., 2012, A&A, 543, 86
Nakano S., 2009, IAU Circ., 9093, 1
Neckel Th., Klare G., 1980, A&AS, 42, 251
Ney E. P., Hatfield B. F., 1978, ApJ, 219, L111
Osterbrock D. E., 1989, Astrophysics of Gaseous Nebulae and Active Galactic Nuclei. University Science Books, Mill Valley, CA
Pavlenko Y. V., Geballe T. R., Evans A., Smalley B., Eyres S. P. S., Tyne V. H., 2004, A&A, 417, L39
Raj A., Ashok N. M., Banerjee D. P. K., 2009, Central Bureau Electronic Telegrams, 2069, 1
Raj A., Ashok N. M., Banerjee D. P. K., 2011, MNRAS, 415, 3455
Romano D., Matteucci F., 2003, MNRAS, 342, 185
Rudy R. J., Dimpel W. L., Lynch D. K., Mazuk S., Venturini C. C., Wilson J. C., Puetter R. C., Perry R. B., 2003, ApJ, 596, 1229
Rudy R. J., Prater T. R., Puetter R. C., Perry R. B., 2009, IAU Circ., 9099, 1
Russell R. W., Laag A., Rudy R. J., Skinner M. A., Gregory S. A., 2010, IAU Circ., 9118, 1
Starrfield S., Truran J. W., Sparks W. M., Kutter G. S., 1972, ApJ, 176, 169
Starrfield S., Sparks W. M., Truran J. W., 1974, ApJ, 192, 647
Starrfield S., Gehrz R. D., Truran J. W., 1997, in Bernatowicz T. J., Zinner E., eds, AIP Conf. Proc. 402, Astrophysical Implications of the Laboratory Study of Presolar Materials. Am. Inst. Phys., New York, p. 203
Strope R. J., Schaefer E., Henden A. A., 2010, AJ, 140, 34
Teyssier F., 2009, AAVSO Alert Notice, 412, 1
van den Bergh S., Younger P. F., 1987, A&AS, 70, 125
Warner B., 2008, in Bode M. F., Evans A., eds, Classical Novae. Cambridge Univ. Press, Cambridge, p. 21
Wichmann R., Krautter J., Kawara K., Williams R. E., 1991, in Jaschek C., Andrillat Y., eds, Proc. Int. Coll., Montpellier, France, The Infrared Spectral Region of Stars. Cambridge Univ. Press, Cambridge, p. 353
Williams R. E., 1994, ApJ, 426, 279
Williams R. E., Hamuy M., Phillips M. M., Heathcote S. R., Wells L., Navarrete M., 1991, ApJ, 376, 721
Williams R. E., Phillips M. M., Hamuy M., 1994, ApJS, 90, 297
Williams R., Mason E., Della Valle M., Ederoclite A., 2008, ApJ, 685, 451
Woodward C. E., Lawrence G. F., Gehrz R. D., Jones T. J., Kobulnicky H. A., Cole J., Hodge T., Thronson H. A., 1993, ApJ, 408, L37
Yaron O., Prialnik D., Shara M. M., Kovetz A., 2005, ApJ, 623, 398

This paper has been typeset from a TEX/LATEX file prepared by the author.